Measuring Particle Size Distributions in Multiphase Flows Using a Convolutional Neural Network

Jan Schäfer, Philipp Schmitt, Mark W. Hlawitschka, and Hans-Jörg Bart*

DOI: 10.1002/cite.201900099

Dedicated to Prof. Dr. techn. Hans-Jörg Bart on the occasion of his 65th birthday

The efficiency of many chemical engineering applications depends on the surface/volume ratio of the dispersed phase. Knowledge of this particle size distribution is a key factor for better process control. The challenge of measurements acquired by optical imaging techniques is the segmentation of overlapping particles, especially in high phase fraction flows. In this work, a convolutional neural network is trained to segment droplets in images acquired by a shadowgraphic approach. The network is trained on artificial images and implemented into a droplet size algorithm. The results are compared to an OpenSource segmentation approach.

Keywords: Convolutional neural networks, Image analysis, Multiphase flows, Particle size distributions, Shadowgraphic imaging

Received: July 09, 2019; *revised:* July 17, 2019; *accepted:* August 08, 2019

1 Introduction

Many processes in chemical engineering involve multiphase flows, where the efficiency is often dependent on the particle size distribution of the dispersed phase. In a liquid-liquid extraction column, a smaller droplet size has a favorable surface/volume ratio, which enables a higher mass transfer but has negative effects on the column hydrodynamics. Due to the small droplet volume, the throughput is limited and the risk of flooding the column increases. In summary, there has to be a trade-off between the particle size and column hydrodynamics during apparatus design and in operation, where knowledge of the droplet size distribution (DSD) plays a major role in process optimization. There are many ways to measure this distribution, e.g., needle and ultrasonic probes as well as optical image processing, all with different advantages and drawbacks [1]. The main problem of optically acquired images is the segmentation of the overlapping objects of interest to assign a diameter to the droplets or particles. An often-used approach for this task is the watershed algorithm [2], which works well for images of low disperse phase fractions, but with increasing clusters of droplets, the segmentation gets worse. This issue can be overcome using a convolutional neural network (CNN), like U-Net introduced by Ronneberger et al. [3]. The network was designed for biomedical cell segmentation – a research field, where the usage of neural networks is well-established.

In this work, U-Net is trained in a segmentation task for chemical engineering applications and implemented into an analysis algorithm enabling a measurement of droplet size distributions. Different from other works, training of the network, which is usually done on already existing database or manually evaluated images, an approach of artificially generated images, is used. This enables a more flexible training of the network on different applications, with different demands, where no databases of evaluated images exist. The combination of trained network and postprocessing algorithm is used to evaluate the droplet size distribution in a multiphase flow of paraffin oil and water using a shadowgraphic imaging approach known as optical multimode online probe (OMOP) [4]. This imaging technique enables an easy segmentation in low to mid phase fractions due to their sharp contrast between particle and background. For higher phase fractions, the lack of information between the boundaries of overlapping particles complicates the analysis of the particle size distribution. The trained CNN provides a solution for better segmentation in these high phase fraction multiphase flows.

Jan Schäfer, Philipp Schmitt, Dr.-Ing. Mark W. Hlawitschka,
Prof. Dr. techn. Hans-Jörg Bart
bart@mv.uni-kl.de
Technische Universität Kaiserslautern, Chair of Separation Science and Technology, Gottlieb-Daimler-Straße, 67663 Kaiserslautern, Germany.

2 Convolutional Neural Networks

Image processing tasks are of major interest across different industries from self-driving cars to augmented reality in industry applications. Convolutional neural networks are designed to solve such visual tasks. Their basic applications are image classification tasks, where a label is assigned to objects in an image, e.g., street sign detection for cars. A digital image represents a large matrix, where each cell is a pixel in the image with values from 0 to 255 in a standard grayscale image. The main idea of CNNs is feature extraction, which is achieved by convolution and pooling operations. Convolution is a linear operation, where the elementwise product of the image matrix (tensor) and a smaller kernel matrix is calculated. The information in the original image is rearranged, using activation kernels to the feature map. Since the kernel cannot overlap the edges of the tensor (Fig. 1), the feature map has a reduced height and width compared to the input. This can be overcome by padding the edges with an extra layer. [5]

The kernels are the learnable parameter in this operation and are adapted in the training of the network. In every network layer, there can be a number of different convolution steps resulting in different feature maps. To the output of the convolution, a nonlinear activation function is applied, here, the most common function is the rectified linear unit (ReLU) operation, which is [5]:

$$f(x) = \max(0, x) \tag{1}$$

The second operation is the pooling of the resulting feature maps. Pooling reduces the dimensions of the feature maps with no learnable parameters. The most common method and the one used in U-Net is max pooling. This extracts small patches from the feature map, for example a 2×2 grid (Fig. 1) and returns the maximum value of this patch as output. [5]

An advantage of U-Net is that it can produce a local segmentation. The output of the network is a segmentation mask, which can be used to analyze images considering the diameter of the segmented object. This is realized by the network architecture of U-Net, which consists of a downsampling path with n layers of convolution and max pooling operations. Each layer can have c different learnable kernels (convolution operations). In the lowest layer of the U-Net architecture, the up-sampling path starts. In this process, the smallest feature map is upscaled to the segmentation mask with the size of the original input image (Fig. 2). This path has also n layers and in each layer learnable kernels.

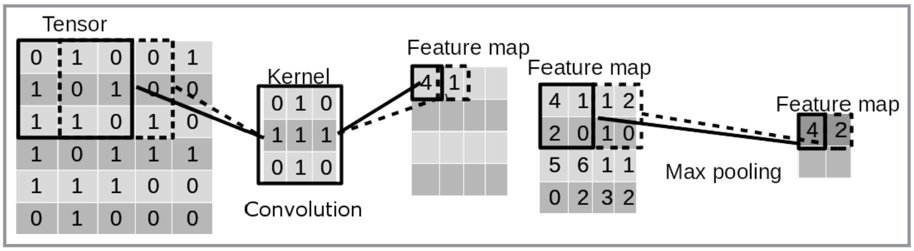

Figure 1. Example for convolution and max pooling operation.

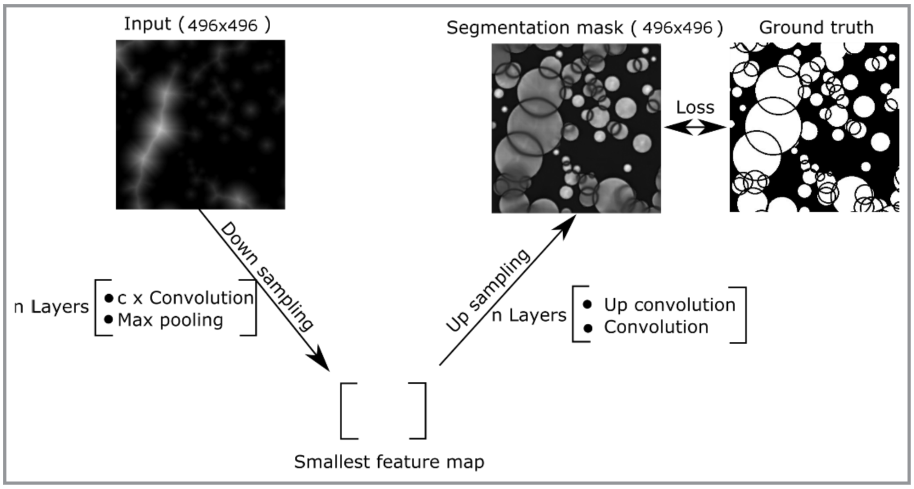

Figure 2. Simplified representation of the U-Net network architecture (for a detailed view see [3]).

For programming and training the network, the Python distribution Anaconda was used, which provides all the needed tools via installable packages and shows very good cross-platform compatibility. All the pre- and postprocessing of the images was done using Python (v 3.6) and the corresponding OpenCV version.

3 Image Acquisition

The setup to acquire the images from the experiments, the OMOP [4], consists of two probes facing each other: a camera (Basler AcA 1300-gm) on one side and an LED for illumination on the other side. The camera uses a telecentric lens, which means only parallel light rays are transmitted to the imaging sensor of the camera. On the illumination side, a plano-convex lens refracts the light emitted from the LED into parallel rays. The advantage of this approach is that the size of an object is independent of the distance to the camera, as long as it is in the depth field of the lens. Also, due to the sharp contrast between the dark projected objects and the bright background, there is a clear segmentation between them. The setup, which was used similar in both experiments, is shown in Fig. 3. The spacing between the two probes can be adjusted for higher phase fractions to minimize the overlapping of particles.

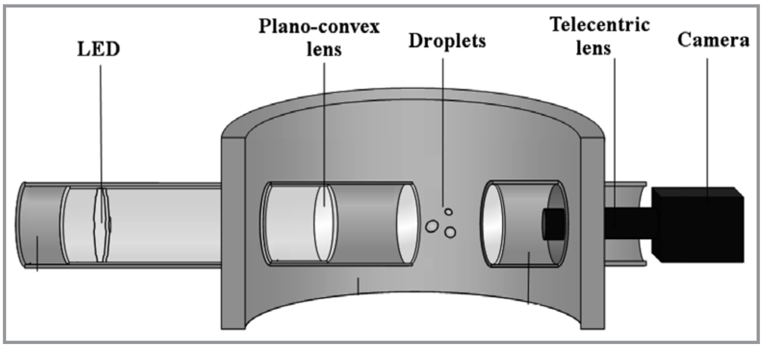

Figure 3. Optical multimode online probe setup.

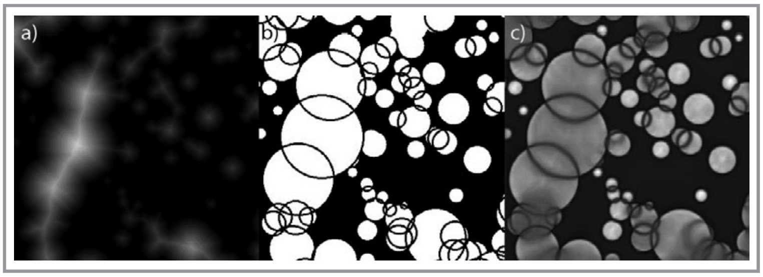

Figure 4. Training sample set: a) input, b) ground truth, c) segmentation map of the CNN.

4 Training Samples

The artificially created images, used for training, need to represent the later acquired images in the experiment that the segmentation is able to work properly. Since the investigated experiments involve liquid-liquid multiphase flows with relatively small droplets, they are assumed to be spherical. The generated images are created by modeling the measuring volume of the OMOP system in three dimensions. In the volume spanned between the two probes, spherical droplets were generated and drawn onto a two-dimensional image, with random positions and size. The droplet size distribution for these images is set to be log-normal distributed. Hold-up, probe distance, mean and the variance of the log-normal distribution can be varied. The final images are drawn as a two-dimensional projection of the three-dimensional measurement zone. The main idea for creating generated images with a good representation of the real experiment is similar to the feature extraction of CNN's. Both, the generated images and the ones acquired in the experiment are preprocessed in a way that only the feature of interest for the segmentation task is used as input for the CNN. Since the droplets are spherical, the most important information about them can be represented using the Euclidean distance transform [6] of the images. This calculates the minimal distance of each pixel to the next boundary pixel, in a binary image. Considering only one droplet in an image, the point with the maximum value of this transformation marks the center of the droplet and the value its radius. An example of this transformation, which was used as input for the CNN can be seen in Fig. 4a.

The following algorithm creates the images, which is used for training the network. In a first step, a random mean diameter m for the particle size distribution is set. The values range between $m \in [0.1,0.3]$ mm, which are the expected values for one of the experiments. The variance is assumed to be 5 % of the mean with $\nu = 0.05m$. With these values, the mean μ and the standard deviation σ of the log-normal distribution were calculated.

$$\sigma = \sqrt{\log\left(\frac{\nu}{m^2}+1\right)} \tag{2}$$

$$\mu = \log\left(\frac{m}{\sqrt{1+\frac{\nu}{m^2}}}\right) \tag{3}$$

$$f(x|\mu,\sigma) = \frac{1}{x\sigma\sqrt{2\pi}}\exp\left\{\frac{-(\log x-\mu)^2}{2\sigma^2}\right\}, \quad \text{for } x > 0 \tag{4}$$

Further, the phase fraction α was varied between 10 and 25 % and the probe distance from 2 to 3 mm. The droplet size distribution, phase fraction, and probe distance were used to create the images by filling the image with randomly chosen circular shapes until the phase fraction in the volume spanned from image height, width, and spacing between the virtual probes was reached. To ensure that the network was not trained on droplets located directly in front or behind other droplets, it was checked if a newly created circle was within a previously drawn circle on the image. This was done by calculating the distance between the centers of the two circles similar to Eq. (6). Is this distance smaller than the sum of the radii, the new circle is disregarded. This is necessary due to the fact that in the experiment droplets in the shadow of other droplets are impossible to detect. The circles on the images are created in two steps. In the first step, all the circles are drawn in white color and filled with no visible boundaries between overlapping shapes. This image is used for preprocessing the input to the CNN. In the second step, only the boundaries of the circles are drawn in black color, so that overlapping circles can be separated correctly. Otherwise, the latest created circle would obscure the older circles. This image represents the ground truth (segmentation mask, Fig. 4b) used as training target for the network. The network is then trained using the distance transform as input and the ground truth as target for calculating the loss function of the training.

5 Training the Network

The database for training the network was created by splitting the 5000 computer-generated images with a resolution of 1280 × 1024 pixel, which matches the resolution of the Basler camera (AcA 1300-gm) into 496 × 496 image segments. The stride size is set to 496 pixels. Consequently, there is no overlapping of the image segments. The database was split into a training and a test set, with a test set size of 10 % of the total images. The used network was set to be 5 layers deep with 5 learnable kernels in each layer, which corresponds to 7 765 442 total learnable parameters The final training of the CNN used the stochastic gradient descent method implemented in PyTorch [7], with a learning rate of 10^{-4}, a momentum of 0.99 and a weight decay of $5 \cdot 10^{-4}$. The training was done on a Nvidia Tesla K80m and completed within two days with a loss on the test batch of 0.18.

6 Postprocessing the Output of the CNN

The final output of the CNN is a segmentation mask (Fig. 4c) which has to be postprocessed for evaluating the droplet size distribution. The segmentations between the different particles are visible as darker lines in the image and the particles are marked as brighter areas. Still challenging are areas with many overlapping particles, where no clear segmentation could be found. Two different approaches were used to overcome this issue, each with different advantages. The first uses the Canny edge detection algorithm [8] to find the edges of the droplets, which are used for the Hough circle transform algorithm to find the particle diameters. The second approach uses a threshold operation to segment the particles into single contours. A simple approach to get the final segmentation of the droplets would be a simple thresholding operation. In this case, the clusters of overlapping droplets, where the predicted boundaries are blurred in the segmentation mask, are not clearly separated and due to the lower pixel values inside the droplets, they might vanish from the final segmentation. This issue is overcome by using an adaptive threshold, in which the value for the threshold is not set globally but locally, in a segment of the image, which strides over the whole image. This resulted in a finer segmentation and enabled a better separation of droplet clusters.

The resulting image (Fig. 5, segmentation image) was then scanned, using a connected component analysis, finding the contours of the separated droplets in the image. Due to the overlapping droplets, the area of single particles is separated, and it is necessary to find the contours that belong together to get the diameter of the droplets in the image. This can be seen in Fig. 5. The box marks a droplet, which gets separated into two different contours by the overlapping larger drop. Humans can easily find the contours belonging to each other by deciding which of them form together a circle. Here, a similar approach was used to fit circles to the contours in the image. The corresponding diameter to the contours was found using the minimal enclosing circle fitted to the area. In a first evaluation step to decide whether the fitted circle was acceptable, the area of the contour (A_c) and the area of the fitted circle (A_{ci}) were compared.

$$R = \frac{A_c}{A_{ci}} = \frac{A_c}{\pi r^2} > 0.7 \tag{5}$$

In this work, decision threshold for this ratio R was 70 %. All circles with a smaller ratio were disregarded. Hence, only single droplets or droplets with a minor overlap were fitted in the first step. The next step was to identify contours, which were enclosed by the same circle. This was done using the extreme points of all the other contours ($P_{e,b}$, $P_{e,t}$, $P_{e,l}$, $P_{e,r}$) on the bottom, top, left, and right edges of the areas. If the distance between the center of the fitted circle and the extreme points of the other contour was smaller than the radius r of the circle, the contour must lie inside the circle.

$$r > \sqrt{\left(x_{ce} - x_{e,i}\right)^2 + \left(y_{ce} - y_{e,i}\right)^2} \tag{6}$$

The area of the contour ($A_{c,n}$) was added to the area of the contour $A_{ci} = A_{ci} + A_{c,n}$ the circle was fitted to in the first place. Subsequently, the same criteria were used for the

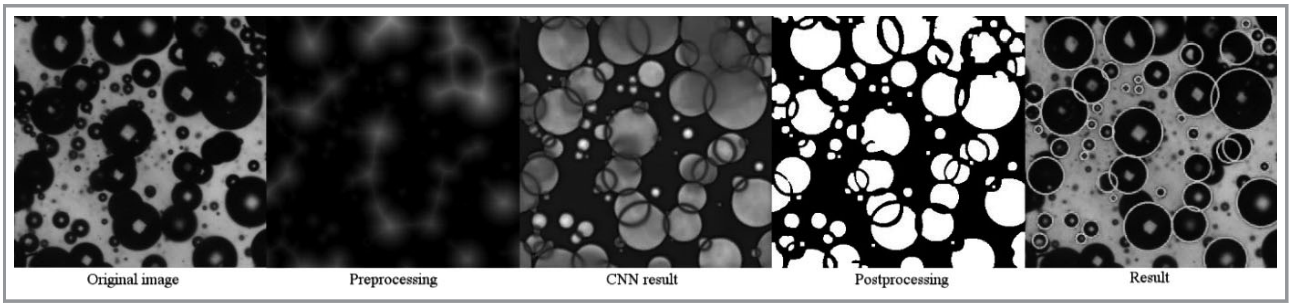

Figure 5. Example evaluation of an OMOP image using the CNN.

area ratio *R* to decide if the fitted circle was good, but with a higher threshold value of 80 %.

7 Preprocessing the Images Captured by the OMOP

Since the network was trained with distance transform images as input, the images acquired in the experiment needed to be preprocessed to match the trained images. Here, the first step was to apply an Otsu threshold to the image, to segment the background from the particles of interest. In a second step, again a connected component analysis was used to get all the contours of the droplets. The center of each droplet is in this case not segmented correctly from the background due to light passing through the droplet. This is corrected by redrawing all contours filled on a blank image. Small imperfections in the acquired images were filtered out in this step. After this, the Euclidean distance transform was applied to the images and they were then used as input for the CNN.

8 Alternative Method: Segmentation Using Watershed

The results of the CNN evaluation are compared to an analysis of the droplet size distribution using the standard tool ImageJ (Fiji [9]). Here, a batch processing script, using the ImageJ Particle Analyzer, evaluates the images taken by the OMOP probe. In a first step, thresholding of the gray scale images will segment them into two classes of pixels. All pixel values smaller than a certain value become the foreground. All pixel values larger than this value are declared as background. Due to the refraction of the parallel-transmitted light at the surface of particles, they get depicted dark on the image sensor. This refraction is low in the center of the particle, which results in a bright spot ("hole") in their middle. In the second step, this hole is filled with the Fill Holes algorithm of ImageJ. Spatial particle overlays are separated with the watershed algorithm because they are imaged on the camera sensor as a common surface. Image width is correlated with the horizontal number of pixels for determination of droplet distributions (1280 pixels/6.8 mm). With the already implemented watershed algorithm of ImageJ and the partial superposition of many particles, lying behind each other, it is not possible to separate all particles completely from each other. For this purpose, only particles with a certain roundness (0.7), the ratio between minimal and maximal Feret diameter, should be evaluated in the automated analysis of particles. The diameter of the droplets is calculated as the area-equivalent diameter.

$$d = \sqrt{\frac{4A}{\pi}} \tag{7}$$

9 Evaluation of the Trained Network

9.1 Validation on Generated Images

Since the pre- and postprocessing algorithms of the images have the potential to falsify the distribution, a first validation step was tested on generated images, where the lognormal distribution was known. For this, the tool for creating the training images was used, but with fixed mean diameter, phase fraction, and probe distance. The results of the CNN were compared to the original distribution and ImageJ evaluation. The result is shown as q_0 distribution of the different measurements in Fig. 6.

The algorithm is able to reconstruct the correct shape of the distribution in every case with the largest deviation on the lower end (100 µm) with a phase fraction of 10 %. Considering the mean diameter of the measured distribution, the average error is 6.4 % for the CNN and 8.9 % for ImageJ.

The next step in the validation process was to generate images with a known monodisperse distribution to evaluate the smallest detectable diameter in the setup with a 1× magnification lens. The phase fraction was set constant to 10 % and the diameter was varied from 20 to 500 µm. Due to the resolution of the image, the measurements on smaller droplets than 80 µm have a high deviation, which is above 10 %. Droplets larger than 90 µm show a maximal deviation of 6.2 % (Fig. 7). As a result, the smallest evaluated diameter in the experiments is set to 100 µm.

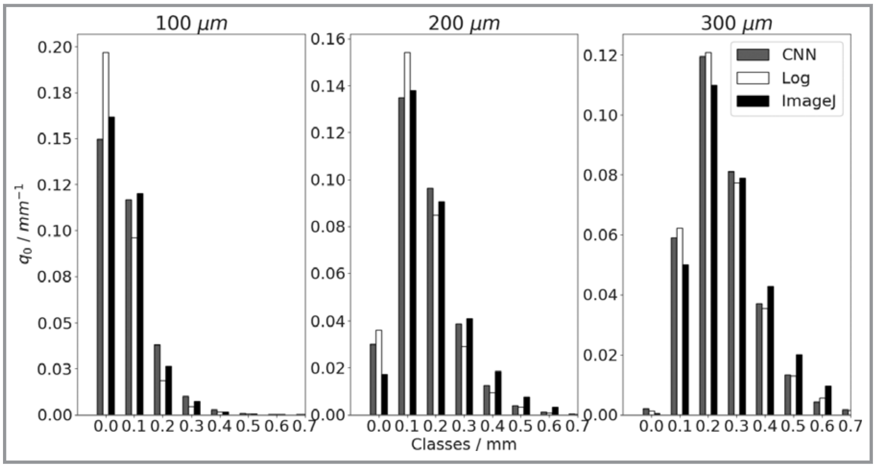

Figure 6. Distribution of generated images and CNN analysis on different mean diameters.

In the last step of the validation process, images were analyzed manually by setting marker points at the droplet edges. Three marker points are then used for fitting a circle. Taken into consideration were only droplets that could be clearly segmented from clusters. A problem of this approach and all the other measurements were smaller droplets. With the used camera lens, with a 1x magnification, particles smaller than 50 µm have a radius of only 10 pixels and are difficult to evaluate properly in the given image material. To evaluate droplets in this range, a lens with a higher magnification is needed.

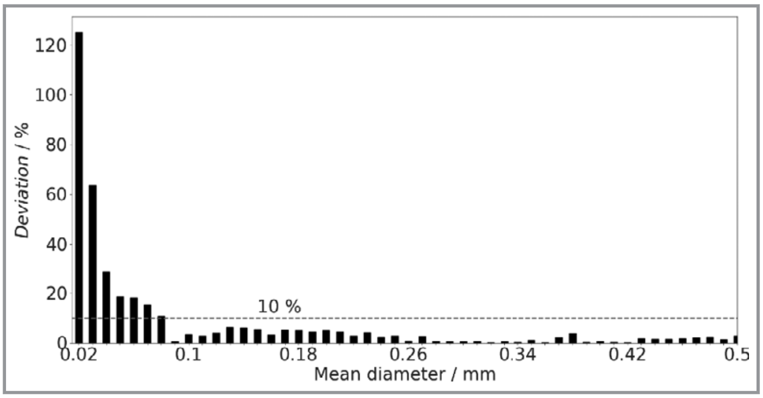

Figure 7. Deviation of measured diameter on generated monodisperse distributions.

9.2 Measurement in Different Applications

The segmentation algorithm using the CNN was tested on two different laboratory setups, a centrifugal pump test rig and a mixer-settler. The two test rigs differ from each other in their dispersing effect. Whereas the mixer settler consists of a classic stirring tank unit and a settler, the dispersion in the pump is generated by the impeller rotation in the pump housing. These two experiments are executed in various DSD ranges, due to different distribution mechanism but using the same substances (paraffin oil/water).

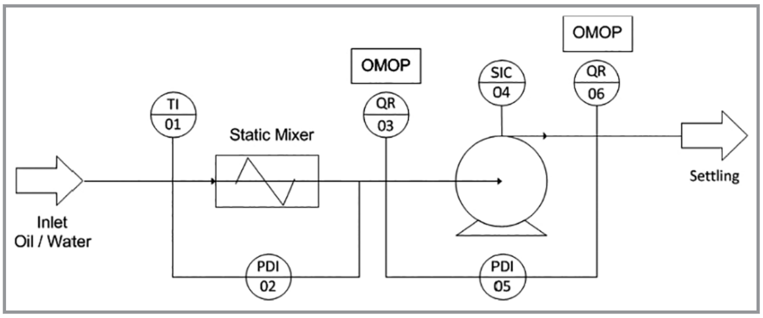

Figure 8. Centrifugal pump test rig.

9.2.1 Centrifugal Pump Test Rig

For experimental dispersion tests, a centrifugal pump test rig was built (Fig. 8). The aim is to investigate dispersion characteristics of centrifugal pumps installed in industrial plants. A radial centrifugal Schmitt MPN 101 pump was used here. The two-phase flow is investigated for variation of flow rate, pump speed, and holdup.

The two-phase flow passes a static mixer (SM) installed in a horizontal pipe. Analysis of the dispersed two-phase flow resulting from the static mixer can be made using pressure difference sensors and an OMOP device. The fluid then flows through the pump, before entering the settler. A secondary OMOP device is integrated into the hydraulic test loop downstream of the test pump.

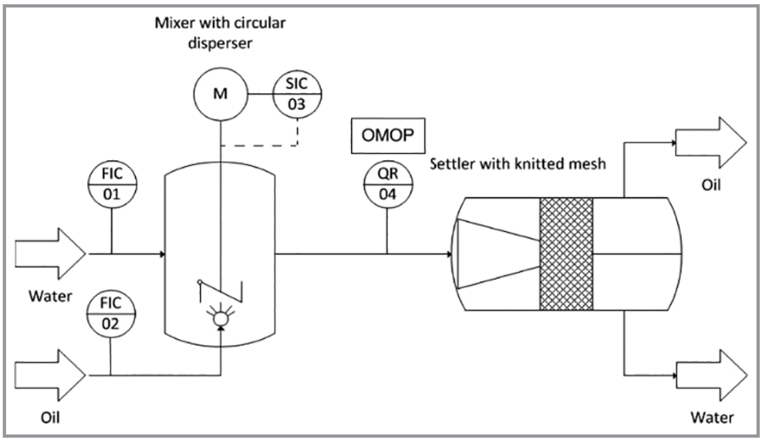

Figure 9. Mixer-settler setup for investigation of knitted meshes.

9.2.2 Mixer-Settler

The second line of experiments are acquired from a test setup to investigate knitted meshes as a coalescing aid in a DN100 mixer-settler laboratory plant (Fig. 9). The two phases, paraffin oil and water, are dispersed in a mixer. At the entry of the settler, the DSD is measured using the OMOP probes.

Different operating points of the centrifugal pump test rig (B1-3) and the mixer settler setup (A1-3) were considered in these experiments. For this purpose, flow rate, phase ratio, and pump/mixer rotation speed were varied (Tab. 1). The measurements of the CNN are compared to the ImageJ and the manual evaluation of the same two images in every experiment (Fig. 10).

The measurements from the pump test rig are in the range of mean diameters the network was trained on. Different to this all, the experiments in the mixer-settler

Table 1. Listing of experiments and results of the image analysis.

Experiment	Flow rate [m^{3}h^{-1}]	Holdup [vol %]	Pump/mixer rotation speed [rpm]	Manual d_{32} (d_{10}) [µm]	CNN d_{32} (d_{10}) [µm]	ImageJ d_{32} (d_{10}) [µm]
A1	0.1	20	250	804 (563)	709 (432)	938 (446)
A2	0.15	20	300	645(436)	668 (450)	620 (376)
A3	0.15	10	250	650 (392)	645 (354)	625 (358)
B1	0.5	1	870	332 (238)	324 (233)	327 (232)
B2	0.5	5	870	384 (269)	360 (261)	394(260)
B3	0.5	10	870	406 (282)	403 (282)	465 (262)

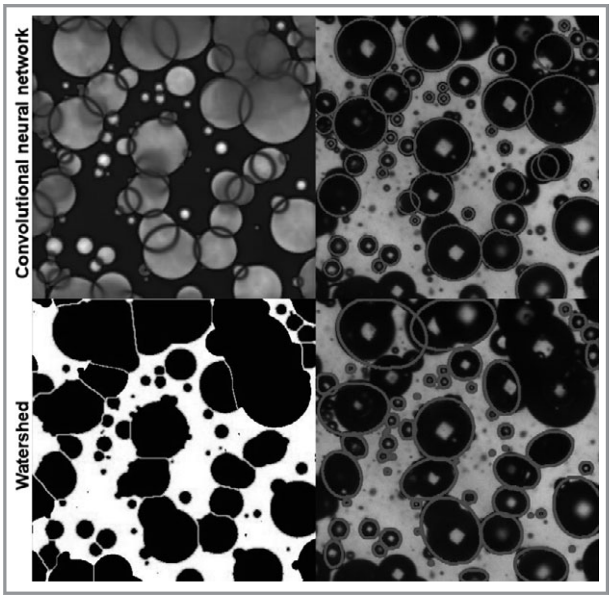

Figure 10. Comparison of the segmentation of CNN (top) and ImageJ watershed (bottom).

have a higher mean diameter. Nevertheless, both evaluations with the CNN show a good agreement with the manual evaluation of the images.

10 Conclusion and Outlook

The trained CNN combined with the algorithm for detecting the droplet diameter shows good results considering the validation with artificially created images. The deviation of the measured mean diameter from generated distributions is in average 6.9 %. Further, the network shows an improvement on the accuracy compared to the open-source ImageJ evaluation in the considered experiments. The mean deviation for the Sauter mean diameter was 4.26 % for the CNN and 11.4 % for ImageJ.

Main advantage of this approach is the flexibility enabled by using generated images for training the network. This allows easy adaption of the CNN on different segmentation tasks in multiphase flows with spherical particles with varying mean diameters of the distribution. The validation showed that droplets below 100 µm cannot be detected properly. This is due to the combination of image sensor resolution and magnification of the camera lens. Larger particles are separated in the preprocessing step, where the image has to be split for the input into the CNN and, thus, are not detected correctly. This is true for particles larger than 500 µm, which corresponds to a third of the input image of the CNN. These problems can be solved partially by using a lens with a different magnification for multiphase flows with a mean diameter near those edges. An adaption of this method for different multiphase systems has to be further investigated. Of main interest are systems with a lower surface tension, with wider DSD, and a higher mean diameter, where not only spherical but also ellipsoidal shapes occur, e.g., bubbly flows. Overall, training a CNN using artificially created images on segmentation tasks enables a flexible adaption of the approach on different applications. In comparison to a segmentation algorithm of ImageJ, a notable improvement in measurement accuracy can be achieved using CNN.

We would like to thank the AiF for sponsoring our research in the two involved projects “Effiziente Tropfenabscheidung an Gestricken” (ERNA) and “Dispergier- und Koaleszierphänomene in Zentrifugalpumpen” (DisKoPump), also we would like to thank the “Regionales Hochschulrechenzentrum Kaiserslautern” (RHRK) for enabling us to use the Elwetrisch Cluster.

Symbols used

A	[µm^2]	area
c	[–]	number of different learnable kernels
d	[µm]	diameter
m	[µm]	mean diameter
n	[–]	number of layers of convolution
P	[pixel,pixel]	point in two-dimensional space
r	[µm]	radius
R	[–]	ratio between two quantities

v	[–]	variance
x	[pixel]	coordinate of a point
y	[pixel]	coordinate of a point

Greek letters

α	[%]	phase fraction
μ	[–]	mean of logarithmic values
σ	[–]	standard deviation of logarithmic values

Sub- and superscripts

b	bottom
c	contour
ce	center
ci	circle
e	extreme points
i	component *i*
l	left
n	component *n*
r	right
t	top

Abbreviations

CNN	convolutional neural network
DSD	droplet size distribution
OMOP	optical multimode online probe
SM	static mixer

References

[1] M. Schlüter, *Chem. Ing. Tech.* **2011**, *83 (7)*, 992–1004. DOI: https://doi.org/10.1002/cite.201100039

[2] *International Conference on Image Processing and its Applications: 7–9 April, 1992, Venue, Maastricht Exhibition and Convention Centre, the Netherlands*, Vol. 354, Institution of Engineering and Technology, London **1992**.

[3] O. Ronneberger, P. Fischer, T. Brox, in *Medical Image Computing and Computer-Assisted Intervention – MICCAI 2015* (Eds: N. Navab, J. Hornegger, W. M. Wells, A. F. Frangi), Lecture Notes in Computer Science, Vol. 9351, Springer, Cham **2015**.

[4] M. Mickler, H.-J. Bart, *Chem. Ing. Tech.* **2013**, *85 (6)*, 901–906. DOI: https://doi.org/10.1002/cite.201200139

[5] R. Yamashita, M. Nishio, R. K. G. Do, K. Togashi, *Insights into Imaging* **2018**, *9 (4)*, 611–629. DOI: https://doi.org/10.1007/s13244-018-0639-9

[6] G. Borgefors, *Comput. Vision, Graphics, Image Process.* **1986**, *34 (3)*, 344–371. DOI: https://doi.org/10.1016/S0734-189X(86)80047-0

[7] A. Paszke, S. Gross, S. Chintala, G. Chanan, E. Yang, Z. DeVito, Z. Lin, A. Desmaison, L. Antiga, A. Lerer, *31st Conf. on Neural Information Processing Systems*, Long Beach, CA, December **2017**.

[8] J. Canny, in *Readings in Computer Vision*, Morgan Kaufmann, Los Altos, CA **1987**.

[9] J. Schindelin, I. Arganda-Carreras, E. Frise, V. Kaynig, M. Longair, T. Pietzsch, S. Preibisch, C. Rueden, S. Saalfeld, B. Schmid, J.-Y. Tinevez, D. J. White, V. Hartenstein, K. Eliceiri, P. Tomancak, A. Cardona, *Nat. Methods* **2012**, *9 (7)*, 676–682. DOI: https://doi.org/10.1038/nmeth.2019